Journal of Applied Physics

Oxide shell layer influences on size-dependent tensile and compressive mechanical properties of iron nanowires: A ReaxFF molecular dynamics study

Cite as: J. Appl. Phys. **126**, 135109 (2019); https://doi.org/10.1063/1.5110363
Submitted: 16 May 2019 • Accepted: 15 September 2019 • Published Online: 07 October 2019

Gurcan Aral

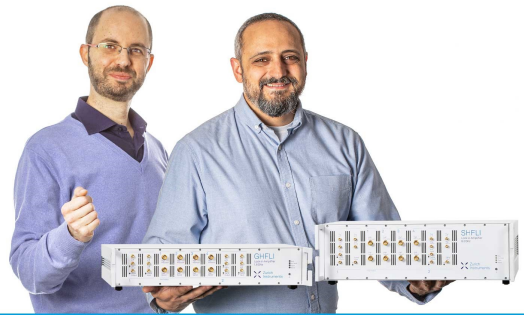

AIP Publishing

Journal of Applied Physics ARTICLE scitation.org/journal/jap

Oxide shell layer influences on size-dependent tensile and compressive mechanical properties of iron nanowires: A ReaxFF molecular dynamics study

Cite as: J. Appl. Phys. **126**, 135109 (2019); doi: 10.1063/1.5110363
Submitted: 16 May 2019 · Accepted: 15 September 2019 ·
Published Online: 7 October 2019

Gurcan Aral[a)]

AFFILIATIONS

Department of Physics, Izmir Institute of Technology, Urla, Izmir 35430, Turkey

[a)]**Author to whom correspondence should be addressed:** gurcanaral@iyte.edu.tr

ABSTRACT

The systematic understanding of an overall deformation mechanism of metallic iron (Fe) nanowires (NWs) with the pre-existing oxide shell layer (Fe/Fe_xO_y) under various mechanical loading conditions is of critical importance for their various applications. Herein, we perform molecular dynamics simulations using ReaxFF reactive interatomic potential to systematically investigate the effect of the pre-existing oxide shell layer on the underlying intrinsic mechanical deformation mechanism and related mechanical properties of metallic [001]-oriented Fe NWs under both uniaxial tension and compressive loading. Three different diameters of the NWs are investigated to elucidate the size effect. The Fe NWs with the preoxide shell layer possess unique and intriguing mechanical properties and deformation mechanisms. In particular, the oxide shell layer with the combined effect of the diameter and the applied uniaxial loading mode dictates the strength and the overall stress-strain behaviors of the NWs. Interestingly, the oxide-coated NWs clearly exhibit the diameter-dependent elastic deformation intrinsic mechanism and related properties as compared to the pristine counterparts. Specifically, the pre-existing oxide shell layer expedites the onset of tensile plasticity by drastically reducing the tensile yield stress and significantly decreasing the tensile elastic limit. Contrary to the tensile loading, the presence of the oxide shell layer reduces or increases the compressive yield stress of the pristine Fe NW with respect to its diameter. However, the pre-existing oxide shell layer leads to a significantly delayed onset of compressive plasticity, that is, a significant increase in the compressive elastic limit.

I. INTRODUCTION

Surface oxidation occurs readily as reactive metallic pristine materials are exposed to a variety of different reactive oxidizer environments.[1–7] As a consequence of the oxidation process, the inevitable formation of a continuous oxide shell layer naturally covers the free surface of metallic reactive materials, depending mostly on the elapsed time, the oxygen pressure, and the temperature of the environment during manufacturing, processing, and working conditions.[1–7] Thereby, physical, chemical, electronic, and mechanical properties of metallic nanomaterials are modified by the oxidation at the free surface.[1–10] The structural evolution containing various defects also takes place around the free surface of materials.[7] Of course, the local defects and thickness of the oxide shell layer become decisive to change the overall properties of nanomaterials, which are distinctive in various degrees from their pristine counterparts.[1–4,8] This offers that pre-existing oxide shell layer effects are inevitable in practical engineering nanoapplications, especially the influence in the mechanical reliability and the environmental performance.[1,11] Therefore, the oxidation mechanisms of nanomaterials and underlying growth properties in various reactive oxidizing environments have attracted significant attention in both experimental and theoretical research studies.[1,2,5–10,12–16]

In fact, the high Fe affinity toward oxygen atoms causes the formation of amorphous oxide shell layers instantly around the metallic core of Fe NW in an oxygen atmosphere.[1–3,7,17] Consequently, metallic NWs are transformed into core and shell (Fe/Fe_xO_y) structures, which exhibit a range of new properties as compared to the pristine NW.[2,7–9] The core/shell (Fe/Fe_xO_y) structure of NWs or the full-oxidized derivative of Fe such as FeO, Fe_2O_3, and Fe_3O_4 associated with a set of unique features has a particular interest as well.[4,8,10,12,15,16] The complex characteristics of

oxide-coated NWs (Fe/Fe_xO_y) including functionality are strongly correlated with the oxide shell layer features such as stoichiometry, phase, local microstructure, thickness, and oxide defects structure, which make Fe/Fe_xO_y NWs as great candidates for highly integrated nanocore/shell structure (Fe/Fe_xO_y) NW devices.[7,8,11,12,15] Therefore, it is of great demand to further research on modulating the overall oxide shell layer properties to achieve the unique properties of the core/shell (Fe/Fe_xO_y) structure of NWs.[8,11] More importantly, understanding as well as predicting the nanomechanical properties of oxide-coated NWs (Fe/Fe_xO_y) is an essential process for obtaining better reliability, optimizing the performance, and, especially, utilizing Fe NWs containing the pre-existing oxide shell layer in various mechanical load-bearing applications.[15]

Numerous studies using molecular dynamics (MD) simulations with fix charge methods have been applied to investigate the mechanical deformation mechanism and related properties of pristine Fe NWs.[18–25] Further, most MD simulation studies for the mechanical response of Fe NWs have been focused on the external variable effects such as size, geometry, crystal orientation, temperature, mode of mechanical loading, strain rate, and defects on the deformation behavior and mechanism in pristine Fe NWs subjected to various mechanical loadings such as tension, compression, and torsion, while ignoring the role of the environment on the mechanical properties.[18–25] Reactive MD simulations with variable charge methods take into account reactive events, which properly incorporate dynamics of charge evolutions including describing bond dissociation and formation between atoms by calculating environmentally dependent charge redistribution through a charge equilibration method.[2–6,13,14,17] Reactive MD simulations with the ReaxFF potentials have provided valuable information on the effect of the pre-existing oxide shell layer on the mechanical properties of the NWs. Despite the importance, until now, only a few MD simulation studies with the ReaxFF potentials exist about the intrinsic role of the pre-existing oxide shell layer on the mechanical properties in metallic NWs such as Fe/Fe_xO_y, Fe/$Fe_xO_yH_z$, Ni/Ni_xO_y, and Al/Al_xO_y NW systems.[2–4,13,14,26] In these studies, metallic NWs with the pre-existing oxide shell layer possess a unique mechanical deformation mechanism and related properties, which are significantly different from their pristine counterparts. Notably, authors have reported that the mechanical deformation behavior and related properties of the metallic NWs such as the thickness of oxide shell layer, the complex local atomistic structure of oxide layer, defects, vacancies, and interface boundaries are highly associated with the extrinsic pre-existing oxide shell layer.

In order to extend our understanding including eliminating uncertainty between theories and simulations, the competing effects between the size and the pre-existing oxide shell layer on the mechanical deformation properties of the pristine and oxidized Fe NWs need to be investigated independently by both simulation and experiments under various mechanical loading conditions. Herein, we perform MD simulations under uniaxial compressive and tensile deformation using the ReaxFF force field for Fe–O systems developed by Aryanpour *et al.*[17] Essentially, the reference paper describes details of the Fe/O/H ReaxFF force field development strategy, including validation data on the mechanical properties of iron and its oxide systems. Previously, the potential has been successfully used to describe the mechanical properties of the Fe/Fe_xO_y NWs.[2,3] The accurate predictions and understanding of the size-dependent deformation mechanisms and related properties of the oxide-coated Fe NWs will be of great interest in the future.

II. DETAILS OF SIMULATION SETUP AND PROCEDURES

We begin with a brief description of the oxidation processes and mechanical deformation simulations. Further details of the simulation setup can be found in our previous works.[2,3,13,14] Starting with a perfect BCC crystalline Fe slab, the cylindrical pristine NWs along the [001] direction with three different diameters but with a same axial length of 14.31 nm are created by removing all atoms outside a cylinder. Three diameters, D = ∼5.0, ∼8.0, and ∼10.0 nm, are considered, and the systems contain a total of 24 050, 61 250, and 95 050 Fe atoms, respectively.

To prepare the formation of the preoxide shell layer, each pristine NW was first relaxed with the conjugate gradient scheme and then thermalized using an NVE ensemble at 300 K.[27] The cylindrical metallic NWs were placed directly in an oxygen-rich environment that consists of 9000 O_2 molecules. The O_2 molecules were randomly placed at 6 A above the free surface of the NW in a vacuum region. The initial velocity of each O_2 molecule is assigned to the temperature of 300 K. Then, we perform MD simulations to oxidize the metallic Fe NWs. Periodic boundary conditions are imposed in all directions during the oxidation process. We observed that the native amorphous oxide shell layer was formed on the free surface of the Fe NWs that have a thickness of ∼1.0 nm. After the formation of the amorphous layer, remaining unreacted O_2 molecules with metallic NW were removed from the simulation box.

To prepare the cylindrical pristine NWs and their oxide-coated counterparts in order to apply the mechanical deformation, each pristine and oxide-coated NW structure was first relaxed to obtain a local minimum energy configuration by using a conjugate gradient algorithm. Then, canonical (NVE) simulations using the Nose–Hoover thermostat were used to thermalize the entire systems at T = 300 K.[27] Equations of motion were integrated with the velocity Verlet algorithm using a time step of 0.5 fs.[28] Prior to the start of mechanical deformation, the systems were further relaxed in isothermal-isobaric (NPT) simulations at 300 K temperature and maintaining zero stress along the z direction.[29] Finally, all NWs were subjected to a constant uniaxial compressive and tensile load with a constant strain rate of 10^8 s^{-1} along the [001] z direction. The systems were maintained at a constant temperature of 300 K using the Canonical (NVT) ensemble with the Nose–Hoover thermostat during the applied mechanical load.[27] A periodic boundary condition was applied along the NW axis to model an infinitely long NW during the mechanical loading. The average engineering stresses in the systems were calculated using the Virial theorem.[28] The Large-scale Atomic/Molecular Massively Parallel Simulator (LAMMPS) was used for all the simulations.[30]

III. RESULTS AND DISCUSSIONS

A. Core-shell (Fe/Fe_xO_y) structural transformation with molecular oxygen in Fe NW

Primarily, the geometrical shape of Fe NWs possesses anisotropy and unique structural characteristics that control the overall

oxidation process. Both experimental and theoretical studies indicate that the chemical reactivity as well as the affinity of O_2 molecule is sensitive to the crystal orientation of the surfaces.[5–7] Once reactive metallic Fe NWs are in contact with the reactive molecular O_2 oxidizing environment, a relatively thin amorphous oxide shell layer is inevitably formed around its free surfaces, which is typically ∼1 nm thick. During the highly complex oxidation process, the growth of the oxide shell layer is strongly correlated with the limited concurrent inward and outward diffusion of O and Fe atoms, respectively. Notably, the diffusion incorporated charge transfer among atoms play an important role in the formation of the oxide shell layer.[2–6] The ionic diffusion rate slows down as the thickness of the oxide shell layer increases primarily due to limited diffusion of reactants to the developing oxide shell region (Fe_xO_y) as well as the (Fe/Fe_xO_y) interface. Consequently, overall ionic diffusions lead to substantial modification of surface states including surface thickness, density, local microstructure, and morphology.[2,3] These fast ionic diffusions both into and out of the free surface reconstruct the regular lattice structure of the metallic core of NW, helping the formation of local defects within the oxide shell layer around the metallic core.[2,7] Thereby, the formation of an oxide shell layer, which inherently induces various surface defects, imperfections, and disordered structure, is associated with the inhomogeneity of the charge states and the amorphous structure.[2,3,7] Potentially, the formation of the oxide shell layer with a nature of oxide surface defects, different complex surface symmetries, inhomogeneities, and imperfection of a local structure due to the oxidation process, results in an increased probability of initial active dislocation sites, which makes the NW more susceptible to activate dislocation motion to onset plastic deformation. Thus, the ability of the disordered oxide shell layer and interface has a significant intrinsic influence on the reduction of the requiring activation stress to onset the tensile plastic deformation and consequently influence plastic mechanical behavior.[2,3] Due to the amorphous nature of the preoxide shell layer, there is also a variation of the local structure and bonding. Namely, the preoxide shell layers are connected to the core of pristine NWs by various chemical and physical bonds. At the nanoscale, such amorphous and inhomogeneous local atomic structural variations may lead to an imbalanced force acting on each atom under the external applied mechanical loads. The chemisorption of O ions to the free surface and further penetration of ionic O atoms into the metallic core during the oxidation process also cause large anisotropic volume expansion on the pristine NWs. Consequently, the generated oxide shell layers expand notably as the diameter of the pristine Fe NWs ranges from ∼5.0, ∼8.0, and ∼10.0 nm to ∼5.9, ∼8.8, and ∼10.7 nm, respectively. The thicknesses of the amorphous oxide shell layers are ∼0.91, ∼0.87, and ∼0.81 nm for the pristine NWs with D = 10.0, 8.0, and 5.0 nm, which correspond to a total number of 4982, 7355, and 8672 O atoms in the amorphous oxide shell layer, respectively.

B. The size effect in pristine NWs

We compare separately the diameter and the preoxide shell layer effects on the mechanical properties of the pristine NWs and discuss one effect independently without considering the other one as well as their coupling effects at the same uniaxial compression and a tensile strain rate of $10^8\ s^{-1}$ at a temperature of T = 300 K. Herein, the pristine Fe NWs subjected to the tensile and compressive loadings are considered as references to compare and highlight the details of the mechanical properties of the oxide-coated counterparts.

First, we discuss the similarities as well as the distinctions of the evolution of the engineering stress-strain curve and demonstrate the corresponding mechanical properties of the pristine Fe NWs as a function of diameters. The elastic stages of the engineering stress-strain curves of the pristine NWs with three different diameters almost overlap in both compressive and tensile mechanical loadings, as shown in Fig. 1. The pristine NWs exhibit a slight size-dependent variation in the strength of NWs in respect to the mode of mechanical loadings. Particularly, it indicates that the diameters have a relatively negligible effect on the yield stress and strain required to onset the plastic deformation under the corresponding mechanical loading. On the other hand, there is a significant distinction in the evolution of engineering compressive stress-strain curves in the plastic region, which indicates that diameter has a strong influence on the compressive plastic deformation behavior for each pristine NWs. Notably, the engineering stress-strain response in the elastic regime becomes less pronounced with the change of NW diameters.

Under compression, the stress increases linearly with the increasing applied compressive strain up to the compressive yield stresses of ∼18.7, ∼17.7, and ∼17.5 GPa at ∼9.5%, ∼9.2%, and ∼9.0% of the corresponding yield strains for D = ∼5.0, ∼8.0, and ∼10.0 nm, respectively. Moreover, the compressive Young's moduli are found as 197.8, 192.5, and 192.0 GPa for the pristine NWs with D = ∼5.0, ∼8.0, and ∼10.0 nm, respectively. Regardless of the diameter, however, stress profiles in all NWs experience a sudden drop after reaching the compressive yield values, which is responsible for the relief of growth stress, indicating the onset of plasticity. Specifically, the onset of plasticity is naturally facilitated by the nucleation of the initial dislocations from the vicinity of the free surface, resulting in the sudden sharp stress drop in both compressive and tensile strains.

Contrary to the compressive loading, the engineering tensile stress-strain curves of pristine NWs show three distinct deformation regions: a linear elastic, a nonlinear elastic, and a plastic deformation regime.[2,3,21] The tensile stress in the nonlinear elastic regime gradually increases with the increasing tensile strains, which is followed by an abrupt stress drop and plastic deformation at relatively lower tensile stresses of 1.1–2.0 GPa. Specifically, tensile plasticity is facilitated by the nucleation of twinning, which results in fluctuation on the tensile plastic stresses. The nonlinear elastic stage is approximately in between strain of 4%–6% (linear yield strain) and 10.2%–10.4% (maximum critical yield strain) at the corresponding stresses in the maximum critical yield stress in a range of 8.2–8.7 GPa, depending on the diameters. The compressive yield stress values of the pristine NWs are ∼2 times greater than that of the tensile yield stress values. Further, it is worth noting that our results show an apparent asymmetry in between the evolution of engineering tensile and compressive stress-strain curves, and the pristine NWs are stronger in compression than in tension. It also agrees well with the compression-tension asymmetry in the plasticity of metallic crystalline Fe nanopillars reported by Healy and

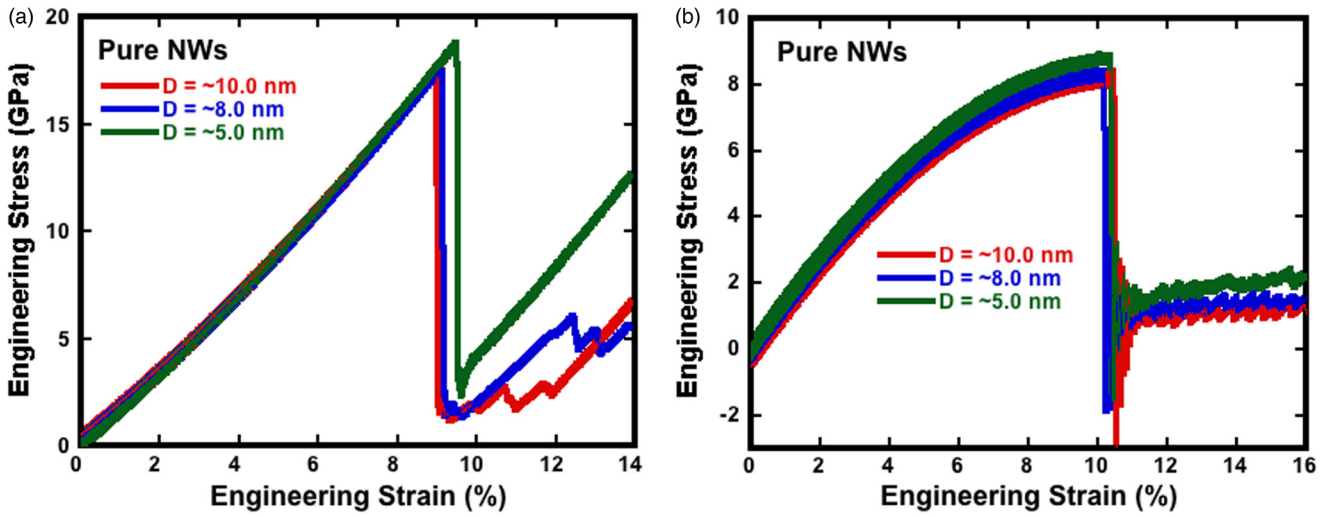

FIG. 1. Characteristic effect of the diameter on the deformation mechanism and related properties, and the average engineering stress-strain curves for the pristine NWs with three different diameters D = ~5.0, 8.0, and 10.0 nm are shown in (a) compressive and (b) tensile loading.

Ackland using MD simulations.[18] It distinctly implies that the pristine NWs can withstand higher external stresses under the compressive loading than that under the tensile loading, due to the relatively higher propensity to dislocation emission from the free surface of NW under the tensile loading. Thus, the pristine NWs that responded to the external applied mechanical loads are coupled with the emission of initial dislocations to the onset of plasticity, depending on the mode of the mechanical loading and the related applied stress and strain level. However, beyond the elastic limit, the variations of the engineering stress-strain curves in the compressive plastic regime are sensitive to diameters.

My results demonstrate that the pristine NWs show a "smaller is *slightly* stronger" trend. Naturally, the "smaller is stronger" trend with the assistance of applied external loads under certain conditions relies essentially on the combined effects of surface states and volume effects, which by themselves would further regularize cooperatively the intrinsic size-dependent properties, increasing or decreasing directly the probability of initiation of dislocation to onset the plasticity.[14] Here, the reasoning above may imply that the available quantities of overall initial dislocation sources including dislocation density and distribution on the free surface of pristine NW and/or the probability of initiation of dislocations to onset the plasticity from the surface of pristine NW with the smaller diameter are essentially to be slightly low, causing a slight increase of the yield stress to onset the plasticity of the pristine NWs.

Our results are consistent with several other previous computational studies. For example, Dutta has studied compressive deformation of the BCC metallic Fe nanopillar oriented in the [001] direction with a 5.8 nm wide square cross section and a length of 15.4 nm, as a function of temperature under a compressive strain rate of $10^8\,s^{-1}$ using MD simulations.[20] He demonstrated that the compressive yield strain and strength of the Fe nanopillar decrease with increasing temperature and reported a linear increase in the compressive yield stress of up to 9.8 GPa at the strain of 8.8% at 300 K. We note that these values are much smaller than our results, due to the potential use of different initial pillar geometries in the simulations. Sandoval and Urbassek studied the role of temperatures on tensile mechanical deformation of the [111]-axial oriented cylindrical BCC Fe NW with D = 3.0 nm using the embedded-atom method (EAM) potential.[21] They revealed that the Fe NWs exhibit two different elastic behaviors, linear and nonlinear elastic responses, only at higher temperatures ($T \geq 300$ K), corresponding to the significant face centered cubic (FCC) and hexagonal-close-packed (HCP) phase transition. Our observation agrees well with the compressive linear elastic behavior reported by Hagen *et al.* from compression tests of α-Fe nanopillars both *in situ* transmission electron microscopy and MD simulations.[22] They performed the uniaxial compression tests on [010] and [011] α-Fe nanopillars at 300 K and 15 K and reported that the deformation can be characterized by initial linear elastic deformation up to a maximum stress peak followed by a decrease in stress. The compressive engineering stress-strain curves indicated a large temperature effect by means of a higher yield and flow stresses when the temperature is reduced. In addition, [011] pillars exhibit the highest strength before yielding in both MD and experiment results compared to the [010] pillars. Our results are consistent with the mechanical deformation behavior reported by Sainath and Choudhary under tension and compression with a constant strain rate of $10^8\,s^{-1}$ at 10 K in the [100] oriented BCC Fe NW with {100} surfaces.[31] They have investigated the influence of the loading mode (tension/compression) on the deformation behavior of Fe NWs using MD simulations employing EAM potential. The stress-strain curves indicate that the [100] oriented Fe NW exhibits significantly higher yield strength under compression than the tensile loading as well as the tension–compression asymmetry.

Unlike compressive deformation, insignificant nonlinearity in the elastic deformation regime is observed under the tensile loading. Moreover, the abrupt stress drop to both the onset of tensile and compressive plasticity is observed. Sainath *et al.* have investigated the deformation behavior and related properties of [110]/{111} BCC Fe NWs under tensile and compressive loading with a constant strain rate of $10^8\,s^{-1}$ at 10 K using MD simulations with an EAM potential.[32] They indicated significant differences in deformation mechanisms and related properties under tensile and compressive loading, indicating the tension–compression asymmetry. However, contrary to our results, they observed that the tensile yield stress is higher than that of the compressive yield stress and the onset of compressive plasticity occurred much earlier than that of tensile plasticity. This suggests that, compared to our results, the deformation mechanisms and related properties of Fe NWs depend on the mode of loading, the orientation of NWs, and temperature. Furthermore, Sainath *et al.* also examined the cross-sectional width (in the range of 1.42–24.27 nm) that is dependent on the tensile mechanical mechanism and related properties in the same system.[24] They reported that the yield stress and Young modules increase rapidly with an increase in size followed by saturation at a larger size. Kim and Greer have carried out experiments to measure the tensile and compressive behavior of single-crystalline BCC molybdenum (Mo) [001]-oriented nanopillars with effective diameters between 250 and 1 μm.[33] They observed a significant difference in the flow stresses between these tensile and compressive deformations in Mo. For example, the flow stresses in tension are lower than those in compression, resulting in attaining only 60% of the compressive flow stresses at 5% strain. Zhang *et al.* have performed MD simulations to study the mechanical response of single crystal Cu with various orientations under uniaxial tensile and compressive loadings.[34] Their studies have revealed a ubiquitous higher compressive yield strength than the tensile yield strength for almost all the investigated orientations, although properties vary significantly with the different crystal orientations. Moreover, they observed an obvious nonlinear stress-strain response in the stage of elastic deformation under applied uniaxial tension or compression, namely, elastic hardening and elastic softening.

C. The size effect in oxide-coated Fe NWs

Next, we examine the diameter-dependent mechanical properties of the oxide-coated Fe NWs with the three different diameters, D = ~5.9, ~8.8, and ~10.7 nm, under the uniaxial tensile and compressive loads similar to the pristine counterparts. On the contrary to the pristine NWs, Fig. 2 reveals that the shape of engineering stress-strain relationships of the oxide-coated NWs shows clear size-dependent strengthening with respect to the diameters. The mechanical properties of oxide-coated NWs are sensitive to the diameters, and the NWs with the smaller diameters are significantly weaker than the larger ones. This is due to the higher quantity of initial overall oxide defects with the reduction of NW diameters. The distinct nature of the pre-existing native oxide shell layer on the free surface of the NW facilitates the initial dislocation sites, lowering the yield stress of the pristine Fe NW with the decrease in diameter. Comparatively, the oxide-coated NWs with the larger diameters possess relatively high yield stresses with an insignificant effect on the yield strain level. As a result, the pre-existing oxide shell layer with the combined effect of the diameter and the applied uniaxial loading mode dictates the strength and the overall stress-strain behaviors of the NWs.

The engineering stress-strain relationship of the oxide-coated NWs in the compressive mechanical deformation displays distinct features as compared to the tensile deformation. Similar to the pristine NWs, the engineering stress-strain curves indicate that the

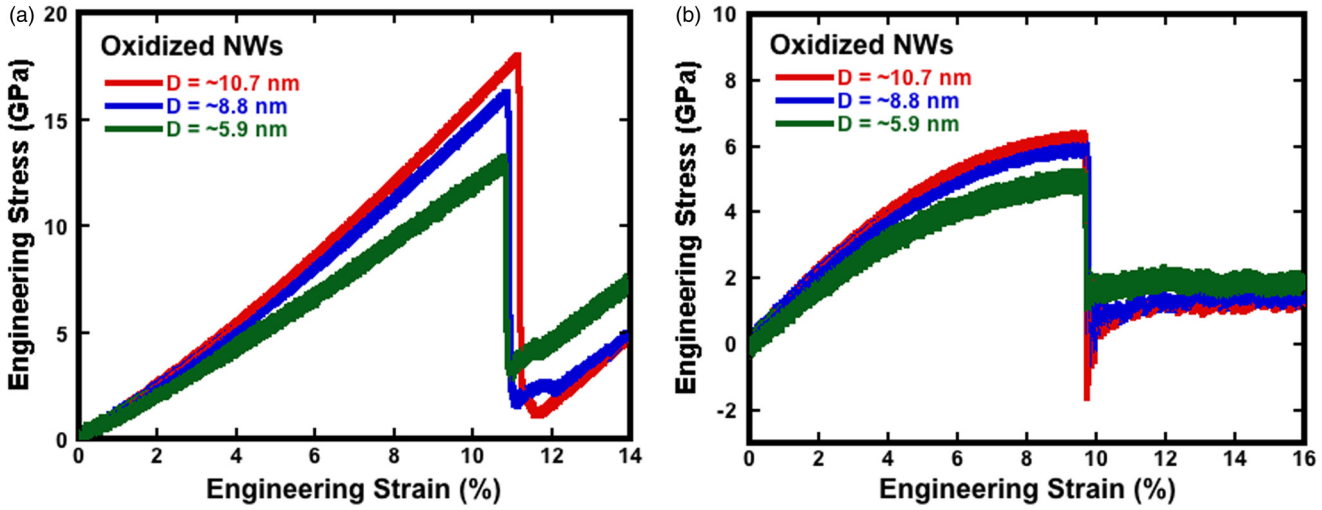

FIG. 2. Characteristic effect of the diameter on the deformation mechanism of the oxide-coated NWs with three different diameters D = ~5.9, ~8.8, and ~10.7 nm shown in (a) compressive and (b) tensile load. The engineering stress-strain curves of the oxide-coated NWs indicate a clear size effect in the yield stress, that is, predominantly related to the pre-existing oxide defects created upon the oxidation process.

oxide-coated NWs have higher yield stresses in the compression loading than that of tension loading, except that the stress level required for the onset of plastic deformation has a different diameter-dependent oxide defects or stress concentrator in respect to the applied mechanical mode. The oxide-coated NWs exhibit a significant reduction in both the tensile and compressive strength of NWs with the decreasing diameter, as shown in Fig. 2. On the other hand, it should be noted that the oxide-coated NWs similar to their pristine counterparts subjected to the compressive loading also exhibit two stages in the stress-strain curve: the linear elastic and plastic deformation stage. For example, the compressive stress increases linearly with the applied compressive strain up to the compressive yield stress value of ∼13.0, ∼16.2, and ∼17.9 GPa at the corresponding approximate strain values of ∼10.8%, ∼10.9%, and ∼11.2% for the oxide-coated NWs with D = ∼5.9, ∼8.8, and ∼10.7 nm, respectively. Notably, the oxide-coated NW with the smaller diameter reaches more easily to its compressive plastic regime. The corresponding compressive Young's modulus values are 161.7, 149.6, and 120.4 GPa, respectively, which decrease dramatically with decreasing diameters of the oxide-coated NWs [see Fig. 2(a)]. The compressive Young's modulus of the oxide-coated NW increases by ∼34% as the diameter increases from ∼5.9 to ∼10.7 nm. We note that these values are lower than Young's modulus for the corresponding pristine counterparts. For example, the oxide shell layer causes a decrement of ∼15.8%, ∼22.2%, and ∼39.1% in the compressive Young's modulus, corresponding to the order of decreasing diameters of NWs.

Likewise the pristine NWs, the oxide-coated NWs also exhibit three distinct stages in the tensile stress-strain curves: linear and nonlinear elastic deformation stages and the plastic deformation stage. During the first initial stage, the tensile stresses increase linearly with the increase of applied strain up to the stress of ∼4.1, ∼3.9, and ∼3.7 GPa at the strain values of ∼5.0%, ∼4.2%, and ∼4.0%, respectively, depending on the diameters. The linear elastic regime is subsequently followed by the nonlinear regime, which is associated with a gradual phase transformation with a continuous increase in stress as the strain increases. The oxide-coated NWs have the tensile maximum critical yield stress values of ∼4.9, ∼5.9, and ∼6.3 GPa at the critical yield strain values of ∼9.7%, ∼9.8%, and ∼9.7%, respectively, with increasing order of diameters.

Due to the lack of experimental studies at the length scale we are studying herein, we could not make a direct comparison with experimental results. For example, Li *et al.* have shown that the surface dislocation nucleation process is highly sensitive to surface stresses that significantly influence the activation processes of surface dislocation nucleation.[35] They have indicated that the activation parameters of surface dislocation nucleation are influenced by the local configurations of surfaces such as local morphology and oxidation layers. This renders size-dependent strengthening or weakening due to the combined effects of surface stress and applied axial stress. In addition to these extrinsic surface conditions and processes, large surface stresses are prevalent in nanoscale pristine metals as a result of the under-coordinated surface atoms. Li *et al.* have investigated the tensile deformation mechanism of Cu-Ag core-shell NWs as a function of shell thicknesses and temperatures using MD simulations with the EAM potential.[36] They have shown that the shell thickness controls the tensile deformation mechanism of the core-shell NWs and, consequently, has significant effects on the mechanical properties. Our observation is consistent indirectly with studies in which pre-existing defects alter the strength of nanomaterials. For example, Wu *et al.* have demonstrated that both surface defects and grain boundary triple junctions serve as effective stress concentrators, which modulates the yield strength of copper (Cu) NWs,[37] and they have highlighted the importance of internal and surface structure effects on the yield strengths of Cu NWs.

D. Comparison of mechanical properties of each pristine Fe NWs and its corresponding oxide-coated counterparts

Herein, a major challenge is to understand qualitatively how, and to what extent, the pre-existing oxide shell layer in the relevant diameter is linked to the mechanical behavior and related properties of the pristine NWs. In particular, we compare each pristine NW to the corresponding oxide-coated counterpart, which enabled us to assess directly the pre-existing oxide shell layer effects on the overall mechanical properties of the pristine NW. The engineering stress-strain curves provide a qualitative comparison of the strength and elastic behavior between the pristine NWs and their corresponding oxide-coated counterparts, as shown in Fig. 3. There is a remarkable difference in the corresponding yield stress and strain between each pair of the pristine and oxidized NWs subjected to both the compressive and the tensile loadings. In addition, our results show an apparent asymmetry in the stress-strain curve including the elastic and plastic regimes in between compression and tension loadings, with NWs and with and without the pre-existing oxide shell layer. The pre-existing oxide shell layer as well as the interface shared by the oxide shell and the metallic core has an intrinsic influence on the yielding behavior and strength of the pristine NW subjected to either type of loading.

The strong mechanical interplay between the metallic crystal core and the oxide shell layer reduces the onset of tensile plasticity at lower yield stress and strain values as compared to the pristine counterparts. Notably, the magnitude of the tensile maximum critical yield stress of the pristine NWs is much larger than that of the oxide-coated counterparts. It indicates that the pristine NWs withstand much higher resistance to onset tensile plasticity than that of the corresponding oxide counterparts. For example, there is a significant reduction in the tensile maximum critical yield stress of ∼23.2%, ∼28.9%, and ∼44.0% for the pristine NW with D = ∼10.0, ∼8.0, and ∼5.0 nm, respectively, indicating that the pre-existing oxide shell layer accelerates the onset of tensile plasticity with the reduction in diameters.

On one hand, our results reveal that the influence of pre-existing oxide shell layer on the compressive yield strain and strain is quite marked as compared to the tensile yield strain and strain. The onset of compressive plasticity occurs at relatively higher compressive yield strains as compared to their pristine counterparts. Therefore, the pre-existing oxide shell layer leads to a significant increase in the compressive elastic limit. Note that the compressive yield strain of the oxide-coated NWs is ∼24.4%, ∼18.5%, and ∼13.7% higher than the pristine counterparts with D = 10.0, 8.0, and 5.0 nm, respectively. The higher compressive yield strain associated with the existence of an oxide shell layer and also diameter

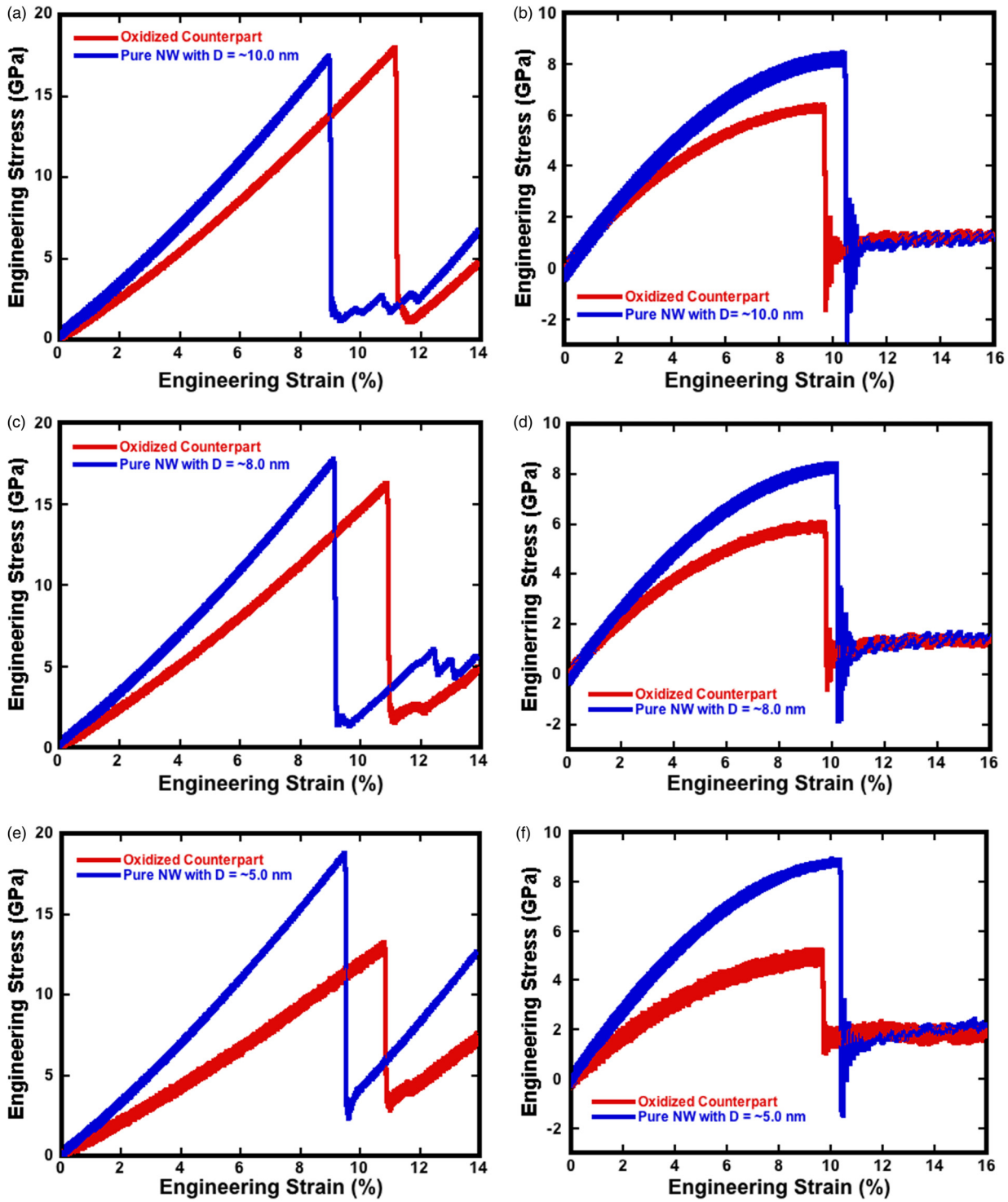

FIG. 3. The quantitative comparison of the average engineering stress-strain curve under compression and tension in between the pristine NW and its oxide counterpart with the pristine [(a) and (b)] D = ~10.0 nm, [(c) and (d)] ~8.0 nm, and [(e)and (f)] ~5.0 nm. Notably, the engineering stress-strain curves indicate that the pre-existing oxide shell layer influences substantially the elastic and plastic deformation mechanism and related intrinsic mechanical properties of the pristine NWs.

delays the onset of compressive plasticity. Comparison of the diameter dependence of the compressive yield stress between the pristine NWs and its corresponding oxide counterparts indicates the onset of compressive plasticity of the oxide-coated NWs, which does not always occur at lower compressive yield stress as compared to the corresponding pristine counterparts. Notably, we observe the compressive softening in the oxide-coated NWs with D = ∼5.9 and ∼8.8 nm. More interestingly, the oxide-coated NW with D = ∼10.7 nm possesses relatively higher compressive yield stress (∼2.3%) than its pristine counterparts. Moreover, the pre-existing oxide shell layer apparently leads to an increase in the compressive yield stress (∼17.9 GPa) comparing with that (∼17.5 GPa) for the pristine counterpart. The activation of compressive plasticity would be relatively difficult with increasing diameter of the oxide-coated NW. In addition to that, the compressive Young's modulus value of the oxide-coated NW with D = ∼10.7 nm is ∼161.7 GPa, which is smaller than ∼192.0 GPa of the pristine counterpart. With the further decrease of diameter, the reduction of the compressive Young's modulus between the pristine NWs and their oxide-coated counterparts are ∼15.8%, ∼22.2%, and ∼39.1%, respectively.

We conclude that the mechanical behavior and related properties of core/shell (Fe/Fe_xO_y) NWs remarkably depend on the pre-existing oxide shell layer, diameter, and the mode of mechanical loadings. The oxide-coated NWs with a smaller diameter encounter small resistance to the onset of plasticity, which supports to lower activation barriers to the onset of plasticity due to relatively small obstacles. Initial sources in the oxide-coated NW typically require relatively much smaller average stress to activate plasticity than its pristine counterpart. On the other hand, the compressive yield stresses are remarkably sensitive not only to the pre-existing oxide shell layer but also to the diameter. Comparatively, the higher strain is required to initiate the onset of compressive plasticity deformation process for the oxide-coated NWs.

E. Compressive elastic deformation mechanism

I have focused and restricted our discussion only to the details of the elastic deformation mechanism. Plastic dislocation analysis in the pristine and the oxide-coated Fe NWs is out of the scope of the present study. Herein, our structural dislocation analyses indicate that the tensile plasticity of all NWs is mainly carried out by twinning including the initiation of twinning, structural transformation such as increases and/or decrease of distance between two twinning planes, subsequent dislocation propagation through the NWs, etc. In our previous studies, we included more detailed discussions on the structural analyses for the tensile plastic dislocation behaviors and mechanism.[2,3] Moreover, the plastic compressive mechanical deformation mechanism of Fe NWs displays unique features that are distinctly different from the plastic tensile one, which is another interesting topic that deserves a separate detailed discussion elsewhere.

The shape of the engineering stress-strain curves of NWs either with or without the oxide shell layer displays that the underlying tensile elastic as well as plastic deformation mechanisms occur very differently than that in the corresponding compressive deformation case. Indeed, it is important to investigate systematically the impact of each contribution on the overall compressive and tensile elastic deformation mechanisms and, especially, to compare their distinctions in details. The influence of oxide shell layers on the elasticity remains largely unclear. Therefore, we first monitor the dynamic evolution of the overall local phase (structural) transformation numbers in the oxide-coated NW with D = ∼10.7 nm that may elucidate the role of the pre-existing oxide shell layer and the underlying physical processes on the overall compressive and tensile elastic and plastic deformation mechanisms. We use common neighbor analysis (CNA) implemented within the OVITO Visualization Tool that enables visualization and the structural characterization of complex defect formation including phase transformation, distribution, and evolutions in the NWs.[38] Dynamic observation of the stochastic local phase transformation evolutions in the compressive elastic regime reveals that atoms in the vicinity of the interface undergo local phase transformations that change nearest neighbor symmetry of atom from the BCC to the FCC phase. Primarily, the FCC phase transformations started to occur roughly at a strain of ∼0.5% and then increased with increasing applied external compressive strain, as shown in Fig. 4(c). However, these FCC phase transformations are concentrated (localized) as well as distributed randomly along the vicinity of the interface shared by the oxide shell and the metallic core with an increasing strain up to ∼7.7%, as shown in Figs. 5(a)–5(f). Notably, the compressive elastic deformation of the oxide-coated NW is correlated spatially and temporally with the local FCC phase transformation with the increasing compressive strain. Up to a strain of ∼7.7%, the inhomogeneous interface between the metallic core and the oxide shell layer with nonuniform morphology evolves in preferable nucleation sites for the FCC phase transformation that may collaborate consistently with the existing anisotropic large local stress concentrations and/or strain under compression. Specifically, the external applied compressive mechanical load may alter the stress concentration (state) along the interface that would have efficiently accompanied by the predominantly inhomogeneous local FCC phase transformations. After the strain of ∼7.7%, the formation of the FCC phase transformation starts to distribute in the interior of NWs with the increasing of the applied compressive strain up to the onset of compressive plasticity. In addition to the BCC-to-FCC phase transformation, when compressive stress reaches its critical value at a compressive stress of ∼14.3 GPa at a strain of ∼9.3%, further compression results in the BCC-to-HPC phase transformation at the interior of the NWs. Importantly, it indicates that the BCC-to-HPC phase transformations have a strong dependence on the compressive stress values. Similarly, most of the studies have revealed that the structural phase transition from BCC to HCP structure starts to occur around 13–14 GPa under compression.[39] The overall number fraction of FCC and HCP phase transformations participating in the compressive elastic deformation mechanism increases with the increasing applied external constant compressive strain up to the onset of plasticity, as seen in Fig. 4(c). Indeed, this suggests that the relatively small emission of the phase transformation from the BCC to the HCP phase contributes less to the compressive elastic deformation. The transformations of FCC and HCP atoms compete and/or collaborate with each other in controlling the overall compressive elastic deformation mechanism. Note that these consecutive phase transformations promote further nucleation dislocations to onset plasticity in the mechanically deformed NWs. Notably, Figs. 4(b) and 4(c) show the rapid increase in phase

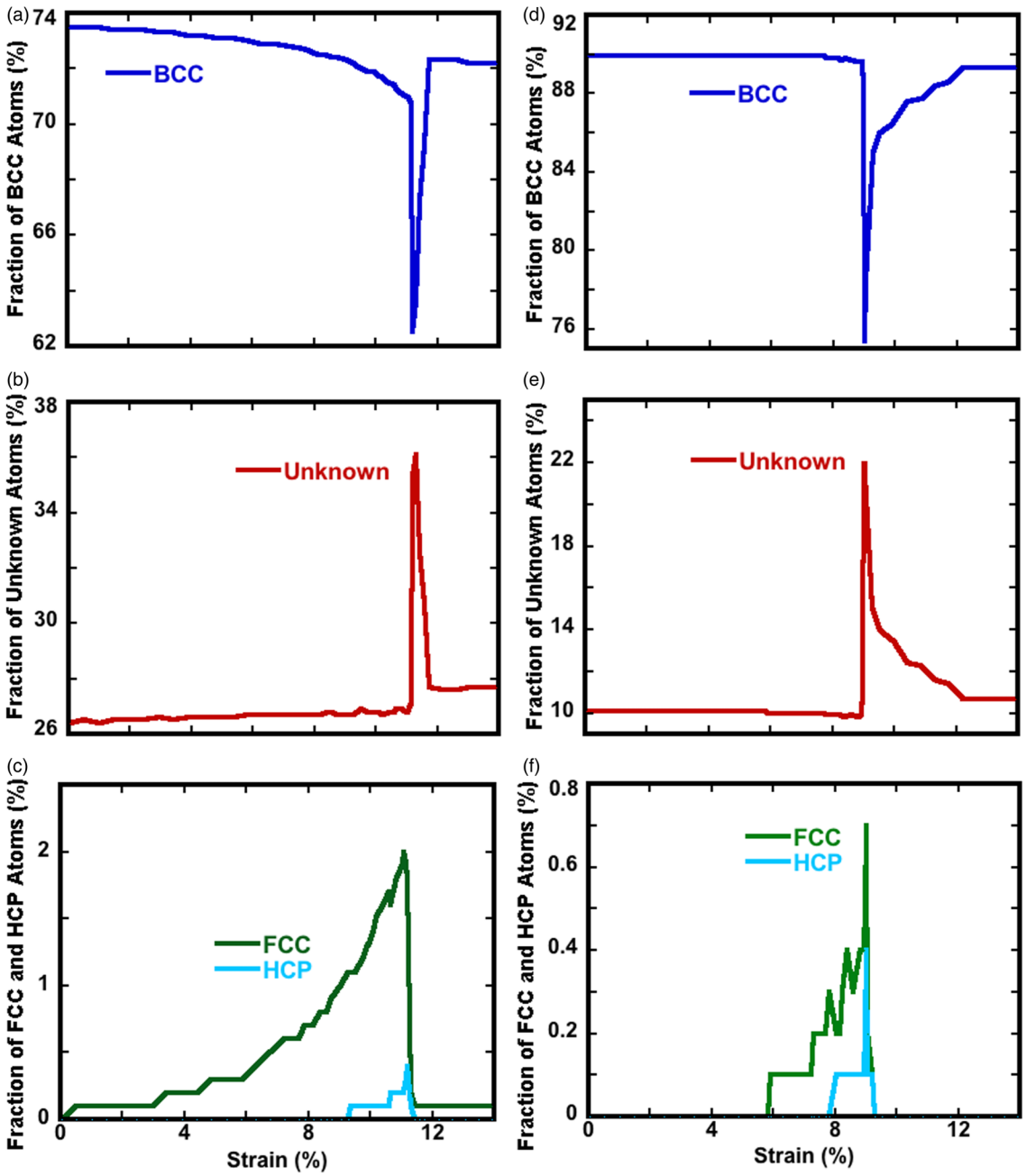

FIG. 4. Temporal evolution of the overall percentage number of atoms with (a) BCC, (b) unknown (other), and (c) FCC and HCP phase transitions in the oxide-coated NW with D = ∼10.7 nm as a function of the compressive strain is shown based on the CNA analysis during the compressive loading. Similarly, the (d) BCC, (e) unknown, and (f) FCC and HCP structural transformation in the corresponding pristine counterpart are also shown.

transformations when closer to the onset of compressive plasticity. However, the majority of the number fraction for FCC and all HCP local phase transformations are rapidly transformed back into BCC and unknown phase transformations, as shown in Figs. 4(a)–4(c). Such rapid transformations are associated with the onset of plasticity, and consequently, the significant stress drops. The FCC and HCP phases are thermodynamically unstable compared with the native BCC phase. Snapshots of the phase transformation and

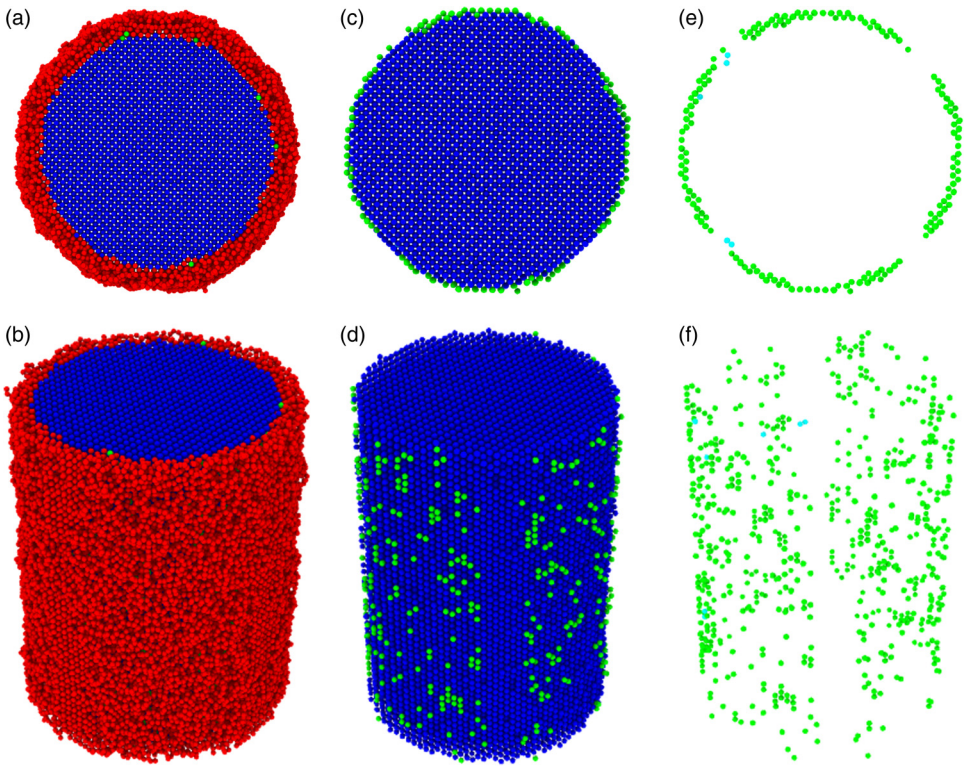

FIG. 5. Snapshots show the oxide-coated NW with D = ∼10.7 nm at the compression strain of ∼7.7%, indicating that the transformation of BCC to FCC ordered atoms concentrate on the interface and distributes randomly along the vicinity of interfaces. It provides some evidence on the pre-existing oxide shell layer effects on the initial elastic compressive deformation activities. The color-coding of atoms with BCC, FCC, HCP, and unknown phase structure is shown based on the CNA analysis as blue, green, cyan, and red, respectively. For the sake of clarity, all unknown structure atoms are not shown in (c) and (f). All FCC atoms are shown in (e) and (f).

distribution in the oxide-coated NW with D = 10.7 nm and its pristine counterpart under compression are presented comparatively in Figs. 6(a)–6(d) and 6(e)–6(h), just before the onset of compressive plasticity. This indicates that the interface helps mainly to accommodate the majority of the overall compressive elastic deformation.

It is found that the compressive elastic deformation behavior of the NWs with and without the pre-existing oxide shell layer has

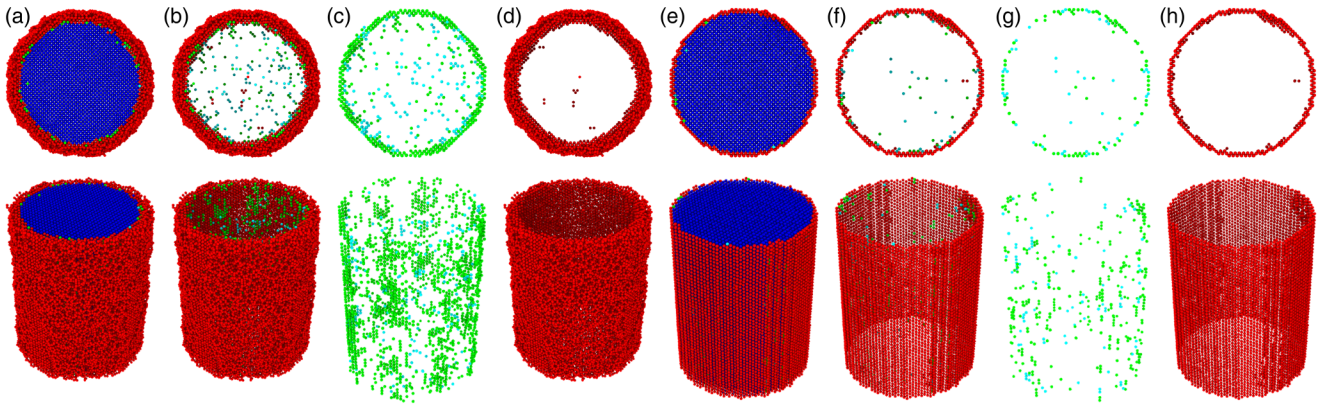

FIG. 6. For comparison, snapshots including cross-sectional and perspective view show the structural transformation in the mechanically strained oxide-coated NW with D = ∼10.7 nm at the compression strain of ∼11.2% [(a)–(d)] and with its pristine counterpart at the compression strain of ∼9.0% [(e)–(h)] just before the onset of plasticity, presenting different patterns of phase transformation network. For comparison, the corresponding structural transformations are shown as the top and side views and were based on the CNA analysis, as blue, red, cyan, and green spheres represent the BCC, unknown, HCP, and FCC lattices, respectively. For the sake of clarity, all atoms with the BCC coordination are not shown in (b) and (f). Moreover, all atoms with the FCC coordination in (c) and (g), and all atoms with unknown coordination are shown in (d) and (h).

different trends, taking likely different propensities for compressive elastic deformation paths, as shown in Fig. 4. The interface and the oxide shell layer play an increasingly vital role during the compressive elastic deformation in the oxide-coated NWs. This is understandable, considering that the initial surface states including the defect levels are very different in between the pristine NW and its corresponding oxide counterpart. Consequently, the contribution of relatively different propensities for the number fraction of phase transformations in the compressive elastic deformation mechanism may be responsible for the observed differences in the size dependence of the yield strength in the pristine NW and its oxide counterpart. Specifically, the occurrence of the compressive elasticity in the oxide-coated NW with D = ∼10.7 nm is accompanied by the formation of a relatively much larger fraction of atoms with FCC phase transformations as compared to its pristine counterpart, as shown in Figs. 4(c) and 4(f). It also indicates that the oxide shell layer facilitates the BCC-to-FCC phase transformations due to the finite size. Also, the oxide-coated NWs are deformed elastically with relatively storing large number fractions of the FCC phase transformation, although the pristine NWs and their oxide counterparts both exhibit very similar compressive elastic deformations localized in the interface. Notably, the oxide-coated NW shows much larger compressive elastic strains, along with strong local phase transformations. Interestingly, the majority of temporal FCC phase transformations occur inhomogeneously and preferentially along the vicinity of the interface region due to a variation of stress values along the length of the NW and/or thermal fluctuations to accommodate the elastic compressive deformation. More importantly, phase transformations from the original BCC to the FCC and HCP structures for the pristine NW with D = 10.0 nm proceeds relatively faster than that of the corresponding oxide-coated NW counterpart. This feature indicates higher rates of structural transformations in the pristine NW than the oxide-coated NW.

F. Tensile elastic deformation mechanism

We further analyze the dynamics structural evolution process of the oxide-coated NW with D = ∼10.7 nm during the linear and nonlinear elastic tensile regimes. Mainly, the external applied constant tensile strain induces the native BCC to FCC and unknown phase transformations that occur preferentially in the interior of the mechanically strained NWs to accommodate the tensile elastic deformation activities. Importantly, the tensile elastic deformation prohibits stress concentration at the interface as increasing the tensile strain, that is, one of the fundamental differences between tension and compression. Namely, the constant external applied tensile strain disperses the induced stress concentration over the overall region of the NW. Primarily, the FCC and unknown phase transformations in the interior of the NW qualitatively describes the overall tensile elastic deformation mechanism, as shown in Fig. 7. Unknown and FCC phase transformations in the interiors of the oxide-coated NWs with D = ∼10.7 nm begin roughly at strain values of ∼3.5% [Fig. 7(b)] and ∼6.1% [Fig. 7(c)], respectively. Then, the number fraction of these transformations increases with the increasing tensile strain and finally reaches the maximum number fraction at a strain of ∼9.7%, which corresponds to the onset of tensile plasticity. Extensive FCC transformations occur in the interior of the NW, where atoms could easily rearrange their structural position by the external applied constant tensile strain, which may be caused by a collaboration of the temporally high stress condition of an atom and/or thermal fluctuations in the ensuing tensile elasticity. Snapshots in Figs. 8(a)–8(d) and 8(e)–8(h) show clearly the structural evolution appearance of the oxide-coated NW with D = ∼10.7 nm and the pristine counterpart just before the onset of tensile plasticity. However, the NW cannot retain the FCC phase transformation structure, which is transformed completely back to BCC and unknown phases when the tensile plastic deformation starts to take place in order to accommodate the external applied tensile uniaxial loading, resulting in the sudden stress drop in the stress in the tensile stress-strain curve of the NWs. Beyond the elastic limit, the BCC-to-unknown phase transformations continue to occur. Atoms with an unknown phase coordination (red atoms) are also associated with the dislocation (stacking faults) nucleation process during the plastic deformation. Similar phase transformation in the interiors of the Fe NWs subjected to the tensile load was observed in our previous MD studies.[2,3]

More profoundly, we found that the tensile elasticity is accommodated naturally by successive high random emissions of the FCC and unknown phase transformation up to the onset of plasticity in the interior of NWs with and without the preoxide shell layer, as shown in Fig. 7. Therefore, the BCC to FCC and unknown phase transformation mechanism controls the tensile elastic deformation of the NWs. Snapshots of the phase transformation before the onset of tensile plasticity show a distinct difference between the oxide NWs and its pristine counterparts, as shown in Figs. 8(a)–8(d) and 8(e)–8(h). However, a comparison of Figs. 7(a)–7(c) and 7(d)–7(f) reveals that the pre-existing oxide shell layer has an obvious influence in changing the tensile elastic deformation paths, which is different from that of its pristine counterparts. For example, the phase evolution in the interior of the oxide-coated NW is relatively different from its corresponding pristine counterpart, where the occurring of elasticity and the onset of plasticity are directly related to the overall phase transformation. Here, the numbers of the unknown and FCC phase structural transformations in the oxide-coated NW are substantially higher than the pristine counterpart. The tensile stress needed to commence tensile plasticity of the oxide-coated NW is relatively lower than the pristine counterpart, owing to the initiation of existing initial dislocations. Notably, the pre-existing oxide shell layer not only affects the overall number fraction but also the evolution speed of the unknown phase transformation without changing the tendency of evolution trend. Moreover, the elastic deformation occurs by storing relatively the large progressive formation of FCC and transformation to unknown structures involved in the tensile elastic processes of NW and, thus, decreases the overall mechanical tensile resistance ability to the onset of plasticity in order to accommodate the external applied tensile strain as compared to the corresponding compressive loading case. The intense FCC and unknown phase transformations' mechanism may be related to the nonlinear elastic deformation behavior of the NWs. The elastic deformation of the oxide-coated NW is dominated partially by a high unknown phase transformation that may likely to be one of the main reasons behind the tensile softening phenomenon, as shown in Fig. 7.

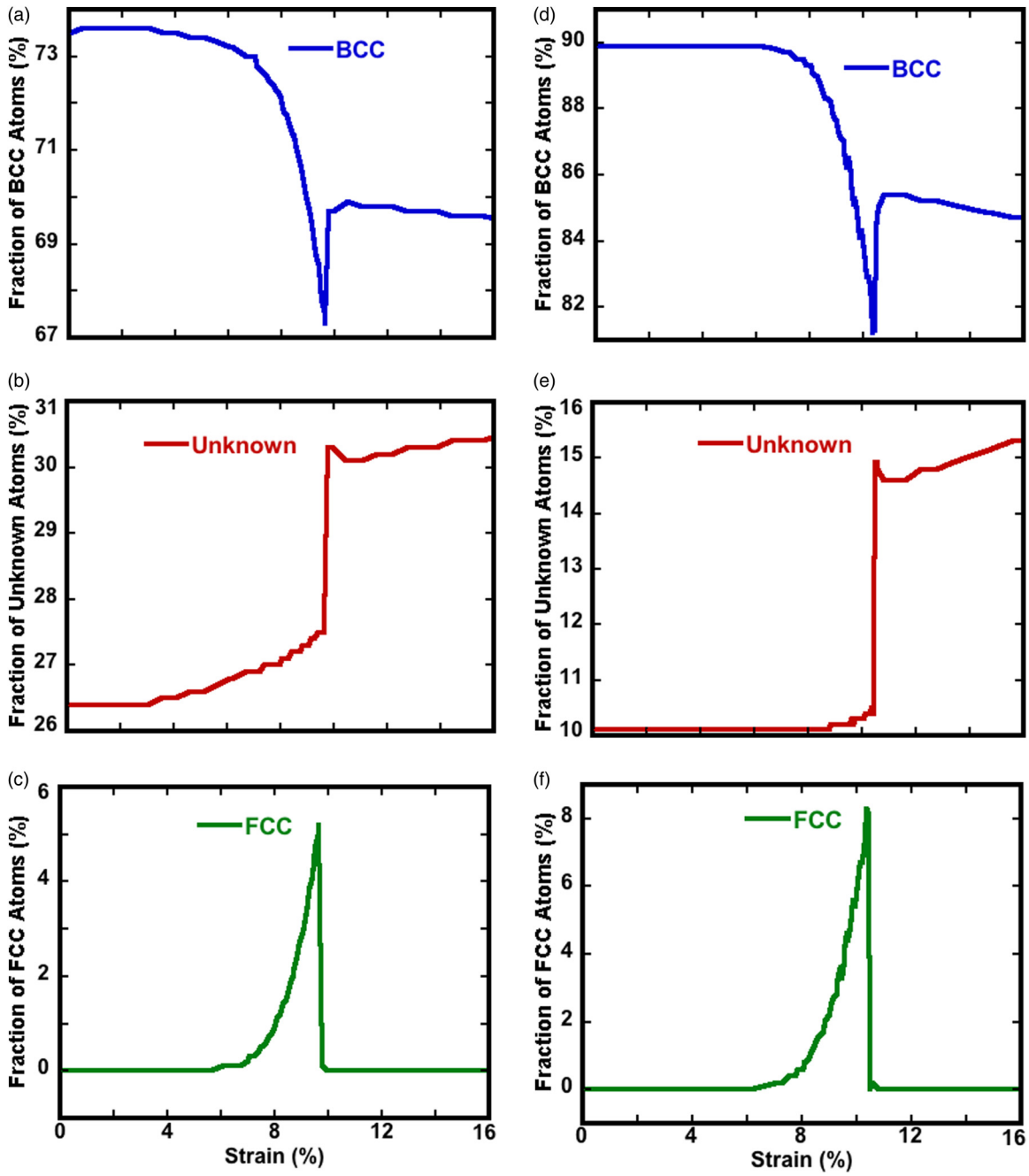

FIG. 7. Temporal evolution of the overall percentage number of atoms with (a) BCC, (b) unknown, and (c) FCC phase transitions in the oxide-coated NW with D = ~10.7 nm as a function of the tensile strain are shown based on the CNA analysis during the tensile load. Similarly, the (d) BCC, (e) unknown, and (f) FCC structural transformation in the corresponding pristine counterpart are also shown.

Some recent studies have investigated the phase transition process in metallic Fe NWs under various modes of mechanical loading. These studies suggest that the mechanical loading modes as well as the crystal orientations have a significant effect on the elastic deformation behavior including the phase transitions. Similarly, Zhu and Shi observed the BCC to FCC and HCP structural transformation for Fe-[110] oriented NWs under compressive loading.[25] Wang *et al.* have investigated the tensile mechanical

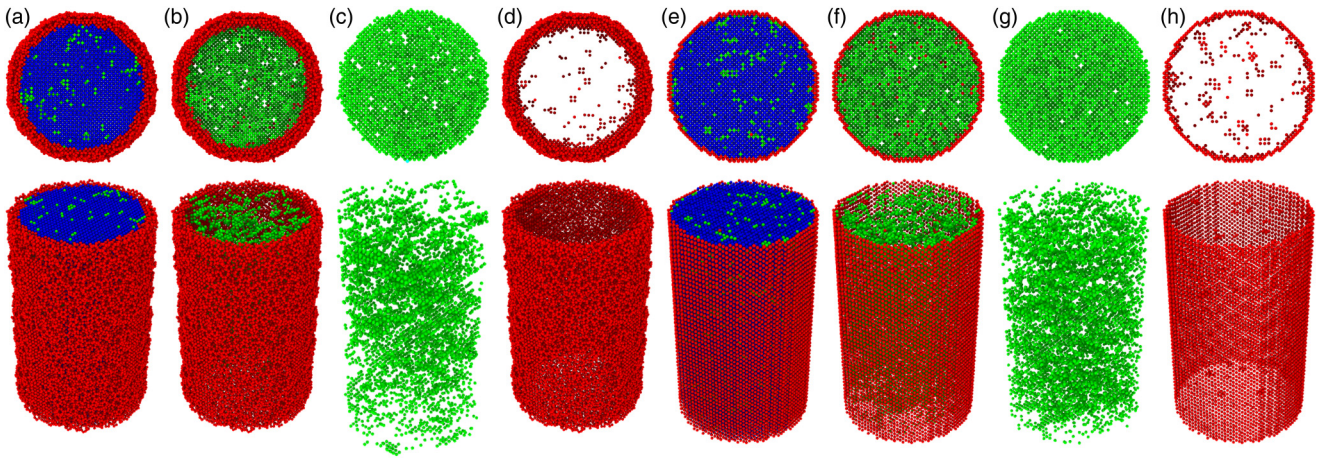

FIG. 8. The phase transformation in the mechanically strained oxide-coated Fe NWs with D = ~10.7 nm at the tensile strain of ~9.7% [(a)–(d)] and with its pristine counterpart at the tensile strain of ~10.4% [(e)–(h)] just before the onset of tensile plasticity. For comparison, the corresponding structural transformations are shown as the top and side views and were based on the CNA analysis, as blue, red, and green spheres represent the BCC, unknown, and FCC lattices. For the sake of clarity, all atoms with the BCC coordination are not shown in (b) and (f). Moreover, all atoms with the FCC coordination in (c) and (g), and all atoms with an unknown coordination are shown in (d) and (h).

deformation of [100] oriented BCC niobium (Nb) NWs by conducting nanomechanical testing using a TEM.[40] They observed the deformation-induced BCC-FCC-BCC phase transformation in the strained Nb NWs. This is discernable since *ab initio* calculation showed that BCC-Nb had two metastable phases of FCC and body-centered tetragonal structures under ultrahigh shear stress.[41] Therefore, the BCC-FCC-BCC phase transformation should be an energetically favored process in Nb NWs. Zolnikov *et al.* have demonstrated that the average lifetime of a single formed FCC atom in the elastic tensile region of the nanosized BCC Fe crystallites is approximately 0.25 fs (one atomic vibration period), due to thermal fluctuation.[42] They have observed BCC-FCC-BCC structural transformations in the tensile elastic stretching region and also in the plastic region. They have pointed out that the fraction of atoms participating in the transformations increases closer to the yield point.

Inherent complexities associated with the native surface oxide shell layer on the free surface of Fe NW lead to different and disproportionate effects on the mechanical elastic deformation behavior of Fe NWs in tension vs compression cases. Primarily, the pre-existing oxide shell layer accelerates the onset of tensile plasticity by lowering the yield stress and strain. In contrast, the pre-existing oxide shell layer provides an additional driving force that leads to a delayed onset of the compressive plasticity, that is, a significant increase in the compressive elastic limit. Additionally, the random local phase transformations occur uniformly through the cross section and along the vicinity of the inhomogeneous interface of the oxide-coated NWs subjected to uniaxial tensile and compressive elastic deformation processes, respectively.

In summary, to study the combined effects of the size and pre-existing oxide shell layer, the remarkable change in the elastic deformation behavior in the pristine NWs and their oxide counterpart coincide with phase transformations, which are the fundamental elasticity carriers, and their interactions with one another and/or with the free surface and the oxide shell layer govern the overall elastic deformation. For example, we observe that the number fraction of phase transformation within the NWs with and without the oxide shell layer proceeds very differently in the elastic stage, as shown in the Figs. 4 and 7. As can be seen from the discussion above, the overall elasticity in the NWs including the nucleation and growth proceeding of the phase transformation is highly sensitive to the existence of the oxide shell layer as well as the mode of mechanical deformation. Notably, it can be seen that the elastic deformation kinetics of the pristine NWs are completely different from their oxide counterpart, due to the presence of a relatively high portion of disordered atoms in the pre-existing oxide shell layer and the interface including a large amount of the defects and imperfections in the preoxide shell layer and the interface. Furthermore, these defects act as the relative potency of stress concentrators, which may lead to modulate the preferred phase transformation sources in the elastic regime. Particularly, the structural transformations, their distribution and the overall number fraction, as well as their interplay in the mechanically strained NWs dictate the overall elasticity of NWs through the coupling of the mode of external applied mechanical load and the pre-existing oxide shell layer. It is worth noting that the phase transformations under tension are proceeded very differently than under compression, as shown in Figs. 4 and 7. Generally, the differences reflect the ease or difficulty of phase transformation and consequently dislocations nucleation at relatively high or low stresses to the onset of plasticity. For example, unlike in the tension, the BCC/FCC phase transformation nucleation sites happen preferably on the interface under the compression, which indicates that the BCC to FCC phase transformation has a strong dependence on the mode of mechanical load. The concentration of phase transformations in the tensile-strained NWs is very different than that in the compressive-strained

NWs, as shown in Figs. 6 and 8. In addition to that, the pristine NWs and their oxide-coated counterparts deform with storing a relatively higher fraction number of the FCC and unknown phase transformation during the compressive elastic deformation than the tensile elastic deformation. It indicates that the FCC phase transformations are relatively easier to be induced under tension than compression. Notably, the NWs are deformed with storing a large number fraction of the FCC phase transformation in a linear and nonlinear elastic manner, lowering the yield to the onset of the tensile plasticity, as to compare to the compressive case. In addition to that, it should also be noted that the atoms nearer to the interface experience a large imposed compressive stress than the interior atoms, which result in taking the place of the majority of the FCC and HCP ordered phase transformation predominantly and preferably along the vicinity of the interface. As a consequence, the occurring process of high phase transformation densities at the vicinity of the interface may result in increasing compressive stress to the onset of compressive plasticity as compared to the tensile stress.

IV. CONCLUSION

In conclusion, we performed MD simulations using ReaxFF reactive force field to investigate the preoxide shell layer effects on the mechanical behavior and related properties of the pristine NWs subjected to tensile and compressive loadings. We demonstrated that the mechanical deformation mechanism and related properties of the pristine NWs in relevant diameter scales are sensitive to the combined influence of the pre-existing oxide shell layer and the diameter and the mode of applied loadings. In oxide-coated NWs, the inevitable formation of the amorphous oxide shell layer on the free surface of the pristine Fe NW is primarily responsible for softening as well as overall mechanical properties of NW with reducing diameters, which is observed during both in the compressive and in the tensile loading. Primarily, the strong and intricate interplay between the oxide shell layer region and the metallic core region is assisted by the external applied mechanical load drive initiation of initial dislocations to onset plastic deformation and thereby contributing directly to the overall intrinsic mechanical deformation mechanism and the related properties of the NWs. The presence of the surface oxide shell layer and the interface acts as easy dislocation sources that reduce the required stress needed to the onset of plastic deformation under both the compressive and the tensile loading for the smaller diameter of NWs.

Further, our quantitative results offer that the surface native preoxide layer remarkably affects the mechanical properties as well as the mechanical strength of metallic Fe NWs under compression or tension that must be considered for practical load-bearing nanoengineering applications, likely implying importance of tolerance regarding the pre-existing oxide shell layer associated with the diameter.

ACKNOWLEDGMENTS

This work was supported by The Scientific and Technological Research Council of Turkey (TUBITAK)-BİDEB 2219 under Grant No. 1059B191400364. Simulations were performed at TUBITAK ULAKBIM, High Performance and Grid Computing Center (TR-Grid e-Infrastructure) and ITU National Center for High Performance Computing (UHEM).

REFERENCES

[1]T. Pan, Chem. Phys. Lett. **511**, 315 (2011).
[2]G. Aral, Y.-J. Wang, S. Ogata, and A. C. T. van Duin, J. Appl. Phys. **120**, 135104 (2016).
[3]G. Aral, M. M. Islam, Y.-J. Wang, S. Ogata, and A. C. T. van Duin, Phys. Chem. Chem. Phys. **20**, 17289 (2018).
[4]F. G. Sen, A. T. Alpas, A. C. T. Van Duin, and Y. Qi, Nat. Commun. **5**, 3959 (2014).
[5]B. Jeon, Q. V. Overmeere, A. C. T. van Duin, and S. Ramanathan, Phys. Chem. Chem. Phys. **15**, 1821 (2013).
[6]R. Subbaraman, S. A. Deshmukh, and S. K. R. S. Sankaranarayanan, J. Phys. Chem. C **117**, 5195 (2013).
[7]M. Krajewski, K. Brzozka, W. S. Lin, H. M. Lin, M. Tokarczyk, J. Borysiuk, G. Kowalski, and D. Wasik, Phys. Chem. Chem. Phys. **18**, 3900 (2016).
[8]W. Zhu, J. Winterstein, I. Maimon, Q. Yin, L. Yuan, A. N. Kolmogorov, R. Sharma, and G. Zhou, J. Phys. Chem. C **120**, 14854 (2016).
[9]A. Ali, H. Zafar, M. Zia, I. U. Haq, A. R. Phull, J. Sarfraz Ali, and A. Hussain, Nanotechnol. Sci. Appl. **9**, 49 (2016).
[10]M. Kaur, J. S. McCloy, W. Jiang, Q. Yao, and Y. Qiang, J. Phys. Chem. C **116**, 12875 (2012).
[11]Z. Ai, Z. Gao, L. Zhang, W. He, and J. J. Yin, Environ. Sci. Technol. **47**, 5344 (2013).
[12]K. Gandha, J. Mohapatra, M. K. Hossain, K. Elkins, N. Poudyal, K. Rajeshwarb, and J. P. Liu, RSC Adv. **6**, 90537 (2016).
[13]G. Aral, M. M. Islam, and A. C. T. van Duin, Phys. Chem. Chem. Phys. **20**, 284 (2018).
[14]G. Aral, M. M. Islam, Y. J. Wang, S. Ogata, and A. C. T. van Duin, J. Appl. Phys. **125**, 165102 (2019).
[15]Y. P. Ivanov, A. Alfadhel, M. Alnassar, J. E. Perez, M. Vazquez, A. Chuvilin, and J. Kosel, Sci. Rep. **6**, 24189 (2016).
[16]L. Yuan, Y. Wang, R. Cai, Q. Jiang, J. Wang, B. Li, A. Sharma, and G. Zhou, Mater. Sci. Eng. B **177**, 327 (2012).
[17]M. Aryanpour, A. C. T. van Duin, and J. D. Kubicki, J. Phys. Chem. A **114**, 6298 (2010).
[18]C. J. Healy and G. J. Ackland, Acta Mater. **70**, 105 (2014).
[19]K. Y. Xie, S. Shrestha, Y. Cao, P. J. Felfer, Y. Wang, X. Liao, J. M. Cairney, and S. P. Ringer, Acta Mater. **61**, 439 (2013).
[20]A. Dutta, Acta Mater. **125**, 219 (2017).
[21]L. Sandoval and H. M. Urbassek, Nanotechnology **20**, 325704 (2009).
[22]A. B. Hagen, B. D. Snartland, and C. Thaulow, Acta Mater. **129**, 398 (2017).
[23]C. Qiao, Y. Zhou, X. Cai, W. Yu, B. Du, H. Wang, S. Wang, and Y. Jia, RSC Adv. **6**, 28792 (2016).
[24]G. Sainath, B. K. Choudhary, and T. Jayakumar, Comput. Mater. Sci. **104**, 76 (2015).
[25]J. Zhu and D. Shi, J. Phys. D Appl. Phys. **44**, 055404 (2011).
[26]F. G. Sen, Y. Qi, A. C. T. van Duin, and A. T. Alpas, Appl. Phys. Lett. **102**, 051912 (2013).
[27]G. J. Martyna, M. L. Klein, and M. Tuckerman, J. Chem. Phys. **97**, 2635 (1992).
[28]M. P. Allen and L. J. Tildesley, *Computer Simulation of Liquids* (Oxford University Press, New York, 1987).
[29]G. J. Martyna, D. J. Tobias, and M. L. Klein, J. Chem. Phys. **101**, 4177 (1994).
[30]S. Plimpton, J. Comput. Phys. **117**, 1 (1995).
[31]G. Sainath and B. K. Choudhary, Comput. Mater. Sci. **111**, 406 (2016).
[32]G. Sainath, B. K. Choudhary, and T. Jayakumar, "Deformation behavior of body centered cubic Fe nanowires under tensile and compressive loading," preprint arXiv:1409.3324 (2014).
[33]J.-Y. Kim and J. R. Greer, Acta Mater. **57**, 5245 (2009).
[34]L. Zhang, C. Lu, and A. K. Tieu, Mater. Lett. **227**, 236 (2018).

[35]Q.-J. Li, B. Xu, S. Hara, J. Li, and E. Ma, Acta Mater. **145**, 19 (2018).
[36]P.-T. Li, Y.-Q. Yang, X. Luo, N. Jin, G. Liu, and Y. Gao, Comput. Mater. Sci. **137**, 289 (2017).
[37]Z. X. Wu, Y. W. Zhang, M. H. Jhon, J. R. Greer, and D. J. Srolovitz, Acta Mater. **61**, 1831 (2013).
[38]A. Stukowski, Model. Simul. Mater. Sci. Eng. **18**, 015012 (2010).
[39]W.-W. Pang, P. Zhang, G.-C. Zhang, A.-G. Xu, and X.-G. Zhao, Sci. Rep. **4**, 5273 (2014).
[40]Q. Wang, J. Wang, J. Li, Z. Zhang, and S. X. Mao, Sci. Adv. **4**, 8850 (2018).
[41]W. Luo, D. Roundy, M. L. Cohen, and J. W. Morris, Jr., Phys. Rev. B **66**, 094110 (2002).
[42]K. P. Zolnikov, A. V. Korchuganov, and D. S. Kryzhevich, Comput. Mater. Sci. **155**, 312 (2018).